CIRP Annals - Manufacturing Technology 00 (2022) 1–4

Contents lists available at ScienceDirect

CIRP Annals - Manufacturing Technology

journal homepage: https://www.editorialmanager.com/CIRP/default.aspx

Predictive model of the surface topography for compliant grinding of brittle materials

Yue Yang, Zhirong Liao (2)*, Zhao Wang

Faculty of Engineering, University of Nottingham, UK

ARTICLE INFO

Article history:
Available online xxx

Keywords:
Finishing
Topography
Compliant grinding

ABSTRACT

During uneven and time-dependent compliant grinding of brittle materials, the surface topography is difficult to predict as ductile and brittle regions are coupled due to compliance occurring in macro/micro tool-workpiece contact. This paper proposed a predictive model for surface topography prediction by considering its ductile-brittle transition in compliant grinding. Shape adaptive grinding and monocrystalline silicon were chosen as an example to validate the proposed model based on progressive grinding tests (spot, line, area). Feed-Spindle Projection Angles are further investigated, revealing that 0° angle can obtain a ground surface with lower area roughness and smaller brittle fragments than 45° and 90°

1. Introduction

Brittle materials play a vital role in optics, semiconductors, instruments, and automotive components. Grinding and other abrasive processes are mostly used on brittle materials removal for obtaining desired surface topography [1]. Even so, brittle fractures are still associated with the material removal process when the load/depth is beyond the critical condition, increasing difficulties in surface topography control.

Compliant grinding shows advantages in improving freeform surface quality by using involved compliant elements (e.g., tool, slurry, abrasive, and tool holder) [2]. The compliance affects the material removal in the macro tool-workpiece contact and micro grain-workpiece interactions. Three stages of grain-workpiece interactions were observed to be distributed from the center to the edge of the footprint under varied contact pressure and cutting speeds in compliant grinding with fixed abrasive grains (e.g., shape adaptive grinding) [3,4]. These previous studies focus on the material removal for a certain dwell time without feed motion [4,5], but very few interests were made in the surface topography investigations with the consideration of compliance.

In compliant grinding of brittle materials (Fig. 1a), such complexities in surface topography prediction are mainly reflected in variable cutting modes (ductile/brittle) depending on diverse local conditions. The complex cutting conditions include (i) uneven contact pressure and speeds in the spot grinding zone (Fig. 1b). This generates uneven material removal depth and affects the cutting modes; (ii) overlapped cutting for a certain dwell time (Fig. 1c). Unequal cutting speeds cause unequal involving numbers of abrasive grains; (iii) accumulation and coupling of uneven contact pressure and speeds under tool feed motion in the time and space domains (Fig. 1d).

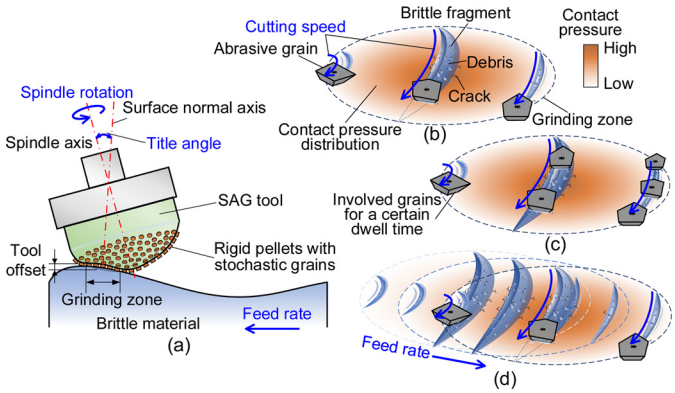

Fig. 1. Compliant grinding of brittle materials (a) showing coupled ductile/brittle removal (b), overlapped cutting for a certain dwell time (c), and the uneven removal accumulation in the time and space domains (d).

In this paper, a predictive model is proposed for investigating the surface topography of brittle materials in compliant grinding. Monocrystalline silicon and Shape Adaptive Grinding (SAG) tools are chosen as an example of brittle materials compliant grinding. The proposed model is able to predict the workpiece surface generation by considering ductile-brittle transition and compliance in SAG This is also further investigated with different Feed-Spindle-Projection Angles (FSPAs), i.e., when the tool feed direction is changed relative to the spindle direction. This work is expected to provide references for material removal mechanisms and processing condition optimization in compliant grinding of brittle materials.

2. Modeling for surface topography prediction

In Shape Adaptive Grinding (SAG) tools (Fig. 2a), pellets are distributed with equal distances between arbitrary adjacent two

* Corresponding author.
E-mail address: Zhirong.Liao@nottingham.ac.uk (Z. Liao).

https://doi.org/10.1016/j.cirp.2022.04.026

Please cite this article as: Y. Yang et al., Predictive model of the surface topography for compliant grinding of brittle materials, CIRP Annals - Manufacturing Technology (2022), https://doi.org/10.1016/j.cirp.2022.04.026

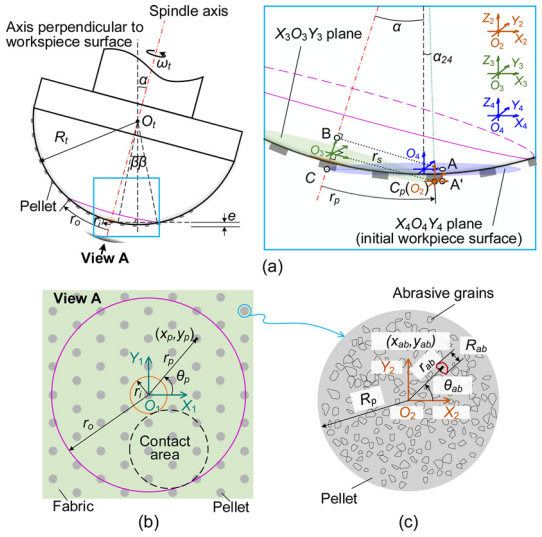

Fig. 2. Shape adaptive tools (a) with patterned distributed pellets (b) and abrasive grains (c).

(Fig. 2b). The pellet center positions can be expressed as () in $X_1O_1Y_1$ coordinate system. It is assumed that the tool head is a perfect sphere and the distances between adjacent pellets are consistent in $X_1O_1Y_1$ coordinate system and over the tool peripheral. The compliance of the tool is assumed to be mainly supplied by the rubber matrix and the deformation occurring in the rigid pellets is neglected. The contact pressure is decreased with material removal, but its distribution manner is consistent.

In each pellet, the abrasive grains (expressed as () in $X_2O_2Y_2$ coordinate system) are randomly distributed as shown in Fig. 2c. Their shapes can be considered spheres while the sizes (R_{ab}) are found to be normally distributed by statistically analysis, as $R_{ab} \sim N(\mu_{ab}, \sigma^2)$. The quantity of abrasive grains on each pellet is around 230. Average abrasive grains diameter (μ_{ab}) is 32 μm, and the standard deviation (σ) is 7 μm.

During grinding, not all abrasive grains on the tool are in contact with the workpiece. The contact area reflecting on the 2D plane is an annular region that depends on the tool tilted angle and tool offset (Fig. 2b). To reduce the computing time, pellets in this region, i.e., $r_i \le r_p \le r_o$, are only considered for the following calculation. r_i and r_o are the inner and outer boundary of the annular region and obtained by assuming that the tool is penetrated the workpiece with the same depth as the given tool offset (Fig. 2a), so that

$$r_{o(i)} = R_t\left(\alpha \pm \arcsin\left(\sqrt{R_t^2 - (R_t - e)^2}/R_t\right)\right) \tag{1}$$

where R_t is the tool radius (including pellet protrusion height), α is the tool tilted angle, and e is the tool offset.

During grinding, with the tool's spindle rotation (ω_t), pellet center positions (x_{p3}, y_{p3}, z_{p3}) can be expressed in the coordinate system $O_3 - X_3Y_3Z_3$, as follows

$$\begin{cases} x_{p3} = R_t \sin(r_p/R_t)\cos(\omega_t t + \theta_p) \\ y_{p3} = R_t \sin(r_p/R_t)\sin(\omega_t t + \theta_p) \\ z_{p3} = 0 \end{cases} \tag{2}$$

Then, pellets center positions (x_{p3}, y_{p3}, z_{p3}) can be transformed to the workpiece coordinate system $O_4 - X_4Y_4Z_4$, so that

$$\begin{bmatrix} x_{p4} \\ y_{p4} \\ z_{p4} \end{bmatrix} = \boldsymbol{T}_{34}\begin{bmatrix} x_{p3} \\ y_{p3} \\ z_{p3} \end{bmatrix} + \begin{bmatrix} -\sqrt{R_t^2 - r_s^2}\sin\alpha \\ 0 \\ R_t - \sqrt{R_t^2 - r_s^2}\cos\alpha - e \end{bmatrix} + \begin{bmatrix} v_{tx}t \\ v_{ty}t \\ 0 \end{bmatrix} \tag{3}$$

where $\boldsymbol{T}_{34}$ is the transformation matrix from the coordinate system $O_3 - X_3Y_3Z_3$ to $O_4 - X_4Y_4Z_4$, and v_{tx}, v_{ty} are tool's feed rates in x and y axes.

For stochastically distributed abrasive grains on each pellet, their position transformation is from the coordinate system $O_2 - X_2Y_2Z_2$ to $O_4 - X_4Y_4Z_4$.

$$\begin{bmatrix} x_{ab4} \\ y_{ab4} \\ z_{ab4} \end{bmatrix} = \boldsymbol{T}_{24}\begin{bmatrix} r_{ab}\cos(\omega_t t + \theta_{ab}) \\ r_{ab}\sin(\omega_t t + \theta_{ab}) \\ 0 \end{bmatrix} + \begin{bmatrix} x_{p4} \\ y_{p4} \\ z_{p4} \end{bmatrix} \tag{4}$$

where $\boldsymbol{T}_{24}$ is the transformation matrix from the coordinate system $O_2 - X_2Y_2Z_2$ to $O_4 - X_4Y_4Z_4$.

The initial workpiece surface plane is set as $z_4 = 0$. When abrasive grains position is below the workpiece surface ($z_{ab4} < z_4$), and grains move into the grinding area ($\sqrt{(x_{ab4} - v_{tx}t)^2 + (y_{ab4} - v_{ty}t)^2} \le \sqrt{R_t e}$, $\sqrt{R_t e}$ is the contact radius), then they interact with the workpiece and generate an updated workpiece surface.

The updated workpiece surface depends on its material removal modes for the chosen monocrystalline silicon. Based on the Preston equation [6], when the material is removed in a ductile mode, the removal depth is

$$h_{dr} = Kp\left|\mathbf{AB}\right|\omega_t \tag{5}$$

$$p = \pi^{-\frac{4}{3}}\left(\frac{3R_p}{4}\right)^{-\frac{2}{3}} D_{sum}^{-\frac{1}{3}} E^* (2E_t)^{\frac{1}{3}}\left(\frac{R_t e - r}{R_t^2}\right)^{\frac{1}{6}} \tag{6}$$

where K is proportionality constant, R_p is pellet radius, D_{sum} is abrasive grains number in per unit area, E^* and E_t are the equivalent Young's modulus and tool rubber Young's modulus, $|\mathbf{AB}|$ is the rotation radius of the abrasive grain (A') around the tool's spindle and varied with the tool's rotation. Based on point A (x_{ab4},y_{ab4},0), point C ($-(R_t - e)\tan(\alpha) + v_{tx}t, v_{ty}t, 0$), and point O_t ($v_{tx}t, v_{ty}t, R_t - e$) positions in $O_4 - X_4Y_4Z_4$ system, $|\mathbf{AB}|$ can be calculated as

$$|\mathbf{AB}| = (|\mathbf{O_tA}|^2 + |\mathbf{O_tC}|^2 - |\mathbf{AC}|^2)/(2|\mathbf{O_tC}|) \tag{7}$$

The removal width is equal to the abrasive grains cross-section width in the ductile mode. When the removal depth (h_{dr}) is beyond the critical plastic-brittle impact depth ($\lambda_{pla-bri}$) [7], the material is removed in the brittle fracture mode. Based on the indentation fracture mechanism [8], the lateral crack depth (C_h) and lateral crack length (C_L) in SAG processes can b achieved as

$$C_h = 0.226(\tan\gamma)^{-\frac{1}{3}}\frac{E_w^{\frac{1}{2}}}{H_v}(p\pi R_{ab}^2)^{\frac{1}{2}} \tag{8}$$

$$C_L = 0.226(\tan\gamma)^{-\frac{5}{12}}\left(\frac{E_w^{\frac{3}{4}}}{H_v K_{IC}(1 - v_w^2)^{\frac{1}{2}}}\right)^{\frac{1}{2}}(p\pi R_{ab}^2)^{\frac{5}{8}} \tag{9}$$

where γ is the semi-angle between two positive edges of an abrasive grain, E_w and v_w are Young's modulus and Poisson's ratio of the workpiece, H_v is workpiece material hardness, K_{IC} is fracture toughness of the workpiece.

Therefore, the removal volume (V_{rab}) for a random abrasive grain can be expressed as

$$V_{rab} = \begin{cases} 2h_{dr}\sqrt{h_{dr}(2R_{ab} - h_{dr})}\left|\mathbf{AB}\right|\omega_t, & \text{in ductile mode} \\ 2C_L C_h\left|\mathbf{AB}\right|\omega_t, & \text{in brittle mode} \end{cases} \tag{10}$$

3. Experiment

To validate the model, dry grinding tests were carried out by using SAG tools (12 mm tool radius, 0.36 mm pellet radius, 1.2 mm distance between pellets' centers) on a CNC machine and grinding forces were measured by Kistler dynamometer 9317 C. The monocrystalline silicon with the orientation of ⟨100⟩ was chosen as the workpiece material with a dimension of 40 × 32 × 5 mm^3. The lapped workpiece surface has an area roughness of 1.1 μm (S_q, root mean square height). To further investigate the material removal mechanism, grinding tests were performed in three levels, including (i) spot grinding, (ii) line grinding, and (iii) area grinding with 15° tilted

Please cite this article as: Y. Yang et al., Predictive model of the surface topography for compliant grinding of brittle materials, CIRP Annals - Manufacturing Technology (2022), https://doi.org/10.1016/j.cirp.2022.04.026

angle, 500 RPM spindle speed, 0.1~0.3 mm tool offset, 5, 10, 15 s dwell time, and 0, 100 mm/min feed rate. For line grinding and area grinding tests, the feed motion is set along the direction with 0°, 45° and 90° towards the tool spindle projected line. The ground workpiece surface topography was measured by an optical 3D measurement system (Alicona G4 InfiniteFocus) with 0.88 μm × 0.88 μm lateral sampling distance, 1429 × 1088 μm^2 field of view. The line roughness was measured in a 5 mm length profile along the feed direction and the area roughness was measured in a 1 × 1 mm^2 area by the MountainsMap Premium without filtering.

4. Model validation and discussion

4.1. Spot grinding

In spot grinding, the tool is held on one spot of the workpiece with no feed motion. It is normally used for obtaining the influence function in the time-dependent material removal processes As shown in Fig. 3a, material removal is increased with dwell time, while the rise between dwell time of 5 and 10 s is faster when the tool offset is 0.3 mm. This is in good agreement with modeling results. The error bars show the measured maximum and minimum values for repeated spot grinding tests (5 times). The increase in material removal with tool offsets (Fig. 3b) under 10 s dwell time corresponds to the increase in tool-workpiece interaction forces (Fig. 3c). To better validate the simulated results, the cross-section for the single spot is collected to be compared with the actual removal profile (Fig. 3d).

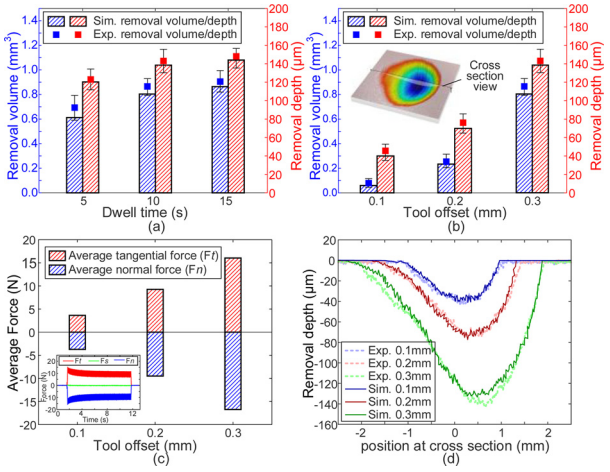

Fig. 3. Modeling and experimental material removal results under different dwell times (a) and tool offsets (b–d).

From the SEM observation (Fig. 5) at different areas in the ground spot (Fig. 4, under tool offset of 0.3 mm), brittle fragments tend to occur in the area under high contact pressure/cutting speeds or both considerations. For example, for areas b, e, h, cutting speeds in areas b and h are slightly higher than area e (Fig. 4a), but brittle fragments are more severe in area e (Fig. 5b, e, h), i.e., the center area of the ground spot, where the contact pressure is higher (Fig. 4a). In comparison between area d, e, f, it has to admit that the pressure (Fig. 4a) and removal depth (Fig. 4b) is higher around the spot center (area e) than the spot edge, but it seems that the area (Fig. 5f) with a higher

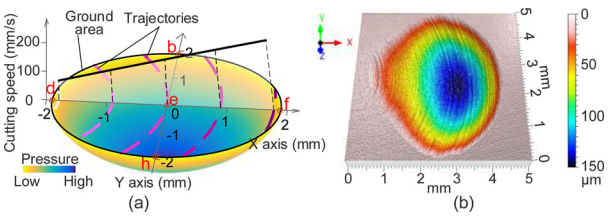

Fig. 4. Trajectory, speed, pressure (a) and material removal (b) distribution in the ground spot.

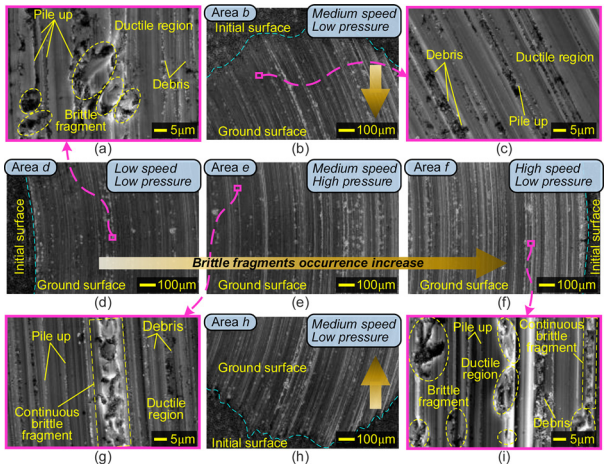

Fig. 5. SEM images of the ground spot measured from different positions (as in Fig. 3) revealing morphology under various speed and pressure (b, d–f, h) with features of brittle and ductile removal (a, c, g, i).

cutting speed (Fig. 4a) has more brittle fragments and less ductile region. This reveals, in such areas, more abrasives are engaged in material removal within the same period, compared with other areas. Cracking generated by the preceding passing by abrasive grains might be extended by the succedent grains at the same speed and pressure. Debris generated from the previous cutting passes further interferes with the follow-up workpiece-grain interactions. These indicate the complexity in the overlapped cutting and uneven removal in spot grinding (without feed motion), and further, reveal the necessity of other validation concerning coupling effects of uneven pressure and speeds (with feed motion).

4.2. Line grinding

The ground groove from line grinding tests can be considered as the integral of the ground spot from spot grinding tests in the time and space domains, and multiple ground grooves form the ground surface with a trench distance. The predicted topography by the proposed model agreed well with the experimental results for all three samples. The removal depth is slightly decreased along the x axis in Fig. 6a. This is because dry conditions may cause some debris to adhere to the tool or remain on the workpiece surface, which slightly changes the tool-workpiece contact. In the comparison of ground grooves under 0°, 45°, and 90°FSPAs, scratches left on the workpiece surface are found to be symmetrical arc (Fig. 6a and d), offset arc (Fig. 6b and e), and along feed direction (Fig. 6c and f), respectively.

These scratches are from the relative trajectories between the workpiece and abrasive grains. Such relative grain-workpiece trajectory distributions affect the material removal together with cutting speeds and contact pressure, which can be well observed in the average cross-section profiles of ground grooves (Fig. 7). Compared with spot grinding (Fig. 5), the approximately symmetrical removal profile from 0° is the accumulated results of spot grinding along its

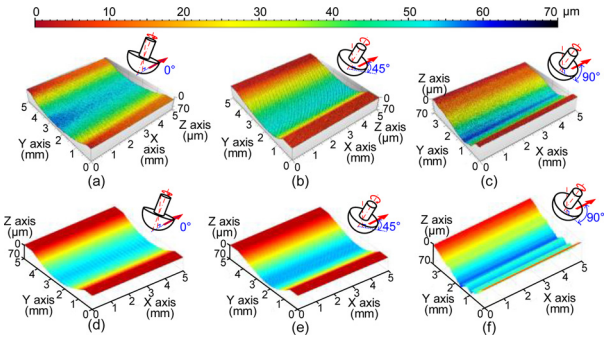

Fig. 6. Comparison in ground surfaces between the experimental (a–c) and simulated results (d–f) under different FSPAs (0°, 45°, and 90°).

Please cite this article as: Y. Yang et al., Predictive model of the surface topography for compliant grinding of brittle materials, CIRP Annals - Manufacturing Technology (2022), https://doi.org/10.1016/j.cirp.2022.04.026

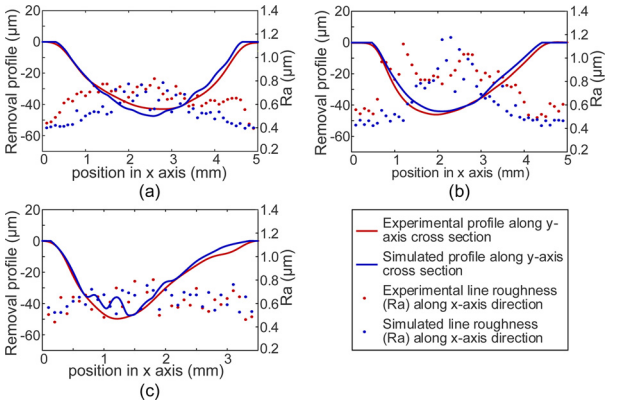

Fig. 7. Groove profile and line roughness in line grinding under 0° (a), 45° (b), and 90° (c) FSPAs.

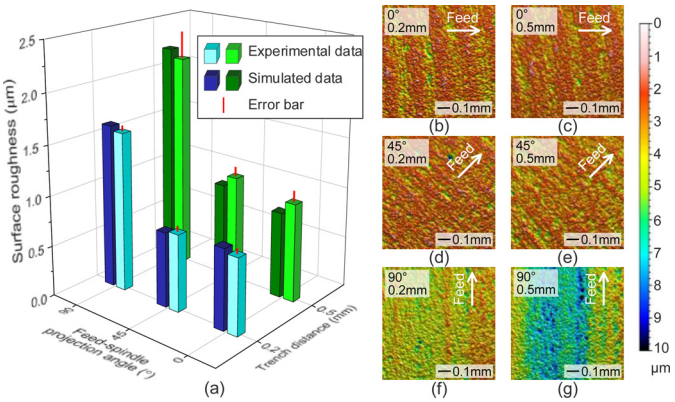

Fig. 9. Area roughness validation between experimental and simulated data (a) and ground surfaces (b–g) from experimental data under different FSPAs (0°, 45°, 90°) and trench distances (0.2 mm, 0.5 mm).

horizontal direction (Fig. 5d, e, and f) in the time and space domains, while the removal profile from 90° is along the vertical direction (Fig. 5b, e, and h). The removal profile from 45° is between the above two cases. However, as for the line roughness along the feed direction in the case of 45°FSPA (Fig. 7b), it is higher than the cases under 0° and 90° (Fig. 7a and c). The differences in line roughness for different positions along grove width (x-axis) are more obvious under 45° than 0° and 90°

SEM images in the area with the deepest removal depth in the groove cross-section show different morphology under 0°, 45° and 90°FSPAs (Fig. 8). Small and dense brittle fragments are observed under 0°FSPA (Fig. 8a), while 45° normally generate relatively large brittle fragments (Fig. 8b). The ductile region in 90° is relatively sharp. To explain this, five uniformly distributed abrasive grains are chosen to simulate and observe trajectory distribution. More trajectory crossing can be found in the case of 45°FSPA (Fig. 8b) than 0° FSPA (Fig. 8a), which induces brittle cutting modes to occur in a relatively bigger area. This causes a relatively higher line roughness along the feed direction (Fig. 7b). For 90°FSPA, more trajectories are overlapped along the feed direction, resulting in repeat cutting supplied by the same group of abrasive grains. Hence, the line roughness along the feed direction is low (Fig. 7c).

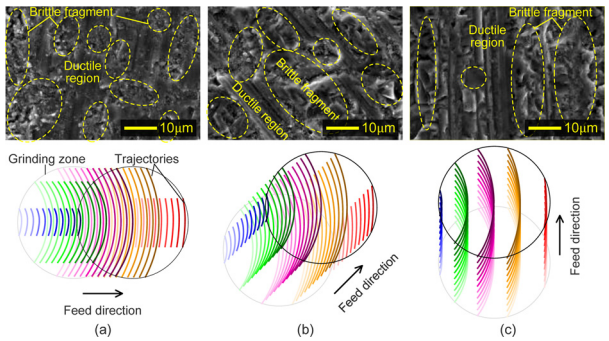

Fig. 8. SEM images and trajectories in the line grinding under 0° (a), 45° (b), and 90° (c) FSPAs.

4.3. Area grinding

For obtaining a ground surface in sub-aperture grinding processes, area grinding is normally performed by multiple line grinding tests with a designed trench distance. From the experimental and simulated data, the area roughness (S_q) under three FSPAs is shown as $S_{q\_90°} > S_{q\_45°} > S_{q\_0°}$ (Fig. 9a). Error bars show the maximum and minimum values of the area roughness (S_q) by measuring different ground areas with the dimension of 1 mm by 1 mm. With the increase of the trench distance, the area roughness is slightly increased under all cases. Compared to line roughness, the area roughness reveals surface quality more comprehensively. It shows that 90°FSPA can generate a ground surface with lower line roughness along the feed direction, but poor surface quality along the direction perpendicular to the feed. From the observation of the ground surfaces (experimental data in Fig. 9b–g), the height variation of the overall surfaces for 90°FSPA is higher than 0° and 45°FSPAs, but the height variation along the feed direction for 90°FSPA is lower (color changes in Fig. 9b–g). This is consent with the observation from Fig. 6. The line roughness is only able to reveal the feature of the surface in the measured direction (i.e., feed direction), but the area roughness presents the feature of the overall surface.

5. Conclusion

This paper proposed a predictive model for the surface topography prediction in compliant grinding of brittle materials. It was validated by spot, line and area grinding tests on monocrystalline silicon with shape adaptive grinding tools at 0°, 45°, and 90°FSPAs. In both experimental and simulated data, the material removal was found to increase with the dwell time and tool offset increase. Brittle modes tend to occur in an area with high contact pressure or high cutting speed. The line roughness along the feed direction in the 45°FSPA case is higher than it in cases of 0° and 90°FSPAs, due to more trajectory crossings. Brittle fragments are smaller and denser in the case of 0°FSPA than others, and sharper ductile regions are observed in the case of 90°FSPA. The area roughness is increased with FSPAs increase for the three chosen cases (0°, 45°, and 90°). While current work focuses on the flate surface, the future work will focus on the convex and concave surfaces grinding.

Declaration of Competing Interest

The authors declare that they have no known competing financial interests or personal relationships that could have appeared to influence the work reported in this paper.

References

[1] Huang H, et al. (2021) Science and Art of Ductile Grinding of Brittle Solids. *International Journal of Machine Tools and Manufacture* 161:103675.
[2] Zhu WL, et al. (2020) Compliant Grinding and Polishing: a Review. *International Journal of Machine Tools and Manufacture* 158:103634.
[3] Zhu WL, et al. (2019) Theoretical and Experimental Investigation of Material Removal Mechanism in Compliant Shape Adaptive Grinding Process. *International Journal of Machine Tools and Manufacture* 142:76–97.
[4] Zhu WL, et al. (2020) Investigation of Critical Material Removal Transitions in Compliant Machining of Brittle Ceramics. *Materials and Design* 185:108258.
[5] Yang Y, et al. (2020) Controlling of Compliant Grinding for Low-Rigidity Components. *International Journal of Machine Tools and Manufacture* 152:103543.
[6] Preston FW (1927) The Theory and Design of Plate Glass Polishing Machines. *Journal of the Society of Glass Technology* 11:214–256.
[7] Bifano TG, et al. (1991) Ductile-Regime Grinding: a new Technology for Machining Brittle Materials. *Transactions of the ASME Series B* 113:184–189.
[8] Lawn BR, et al. (1980) Elastic/Plastic Indentation Damage in Ceramics: The Median/Radial Crack System. *Journal of the American Ceramic Society* 63(9–10):574–581.

Please cite this article as: Y. Yang et al., Predictive model of the surface topography for compliant grinding of brittle materials, CIRP Annals - Manufacturing Technology (2022), https://doi.org/10.1016/j.cirp.2022.04.026